



## Numerical Simulation of 3D- Flow Structure and Heat Transfer for Longitudinal Riblet Upstream of Leading Edge Endwall Junction of Nozzle Guide Vane

Prof.Dr.Najdat Nashat. Abdulla  
College of Engineering  
E-mail najdat\_abdulla@yahoo.co.uk

Asst.Prof.Dr.Ikhlas Mohammed Fayed  
University of Technology  
E-mail ikhlase 60 @ yahoo. com

Asst .Lecturer Kareem Khalf Ali  
Technical Instituted-Baquba  
E-GEml Kareemkhalf72@Google .com

### ABSTRACT

The simulation have been made for 3D flow structure and heat transfer with and without longitudinal riblet upstream of leading edge vane endwall junction of first stage nozzle guide vane .The research explores concept of weakening the secondary flows and reducing their harmful effects.Numerical investigation involved examination of the secondary flows ,velocity and heat transfer rates by solving the governing equations (continuity , Navier -stokes and energy equations ) using the known package FLUENT version (12.1).The governing equations were solved for three dimentional, turbulent flowe, incompressible with an appropriate turbulent model ( $k-\omega,SST$ ) .The numerical solution was carried out for 25 models of V-groove riblet with wide ranges of height (h) and space (s). The results indicated that, the riblet endwall junction was a powerful tool for controlling the flow structure , reducing secondary flow formation,and elimination the effect of heat transfer at leading edge and passage . The drag reduction produced by riblet was proportional with their height and space. V-groove riblet with dimension of (h=1.35mm and s=2.26mm) was found to be the most effective in reduction of drag (2.7%) and heat transfer (21%) so it was selected as an optimum dimension of riblet model. The results also showed that the drag reduction produced by riblet was proportional to their size. The riblet model had a great effect in elimination spanwise ,pitchwise velocities ,but strength the streamwise velocity .At leading edge ,the effect of secondary flow was extended up to 23% from span height and 35% upstream leading edge .The riblet model caused an increase in momentom at a region very close to leading edge and to move stagnation point very close to the leading edge.

المحاكاة العددية لتركيب جريان و انتقال الحرارة ثلاثي البعد وباستخدام حزوز طولية في مقدمة اتصال الحافة الامامية لريش التوربين الثابتة

م.م كريم خلف علي

أ.م.د أخلص محمد فياض

أ.د نجدت نشأت عبد الله

### الخلاصة :

تم اجراء التحليل العددي لجريان ثلاثي الابعاد و لانتقال الحرارة و لحالتي وجود و عدم وجود الحزوز الطولية في مقدمة الحافة الامامية للريش الموجه الثابتة و للمرحلة الاولى . البحث الحالي إستكشف طريقة لإضعاف الجريان الثانوي و يُخَفِّضُ تأثيراتهم الضارة . تضمن التحليل العددي اختبار الجريان الثانوي و السرعة و معدل انتقال الحرارة من خلال حل المعادلات الحاكمة (الاستمرارية و نافيرستوك و الطاقة ) باستخدام البرنامج الجاهز ( FLUENT ) اصدار ( ١٢,١) . تم حل المعادلات الحاكمة بثلاث ابعاد و لجريان مضطرب و لانضغاطي و باستخدام نموذج اضطراب ( $k-\omega,SST$ ) . شمل الحل العددي ٢٥

نموذج للحزوز ولمدى واسع للارتفاع (h) والخطوة (s). النتائج المستحصلة تشير ان الحزوز في منطقة الاتصال تعمل كاداة فعالة للسيطرة على الجريان والتقليل من الجريان الثانوي والحد من تأثير درجة الحرارة عند الحافة الامامية للريشة وكذلك الممر. ان انخفاض الكبح المتحقق بوسطة الحزوز يتناسب مع الارتفاع والخطوة للحزوز. ان النموذج ذو البعد (h=1.35mm) و (s=2.26mm) كان الاكثر تأثيرا في خفض الكبح بمقدار (2,7%) والحرارة (21%) لذلك تم اختياره كافضل نموذج للحزوز. تشير النتائج ايضا الى ان الحزوز الطولية فعالة جدا في تقليل مركبات السرعة العرضية باتجاه الارتفاع والخطوة ولكن تزيد من مركبة السرعة المحورية. عند الحافة الامامية كان تأثير الجريان الثانوي يمتد الى (23H%) وكذلك (30C<sub>ax</sub>%) قبل الحافة الامامية للريش. والحزوز ايضا تزيد الزخم في المنطقة القريبة جدا من الحافة الامامية وتحرك موضع نقطة الركود الى نقطة اقرب الى الحافة الامامية.

## 1.INTRODUCTION

The flow at endwall junction is very complex and it is well known that three - dimensional secondary flows in endwall junction of inlet guide vane can dramatically affect the performance of gas turbine. Consequently, there is a strong need for computation model/tools that would allow an accurate prediction of the secondary flow effect on both the pressure losses and heat transfer. Recent advances in flow control have the potential for significant impact on the design and performance of modern gas turbine engines, weakening secondary flow, delaying separation, reducing drag and creating virtual shape with modifying.

The present work focus on riblet of longitudinal groove with streamwise direction locates before the leading edge of airfoil as shown in **Fig. 1**. There are two types of flow control technique, active and passive. Active flow control method requires an energy input such as suction or blowing to delay transition and modify the fluid viscosity with polymers and film cooling. While the passive control method not require energy and it is a low cost method such as a longitudinal riblet ,leading edge fillet and three dimension contour endwall junction.

A number of researches had investigated endwall modification in the past .As a tool of reducing secondary flows and losses, many techniques have been approved numerically to pursue drag reduction. To create a method of horseshoe vortex reduction elimination, first it is necessary to understand the reason for the formation of the vortex. **Sieverding , 1985**, gave a comprehensive review of the secondary flow structure which produce losses in several ways : first of these flows is the extraction of energy

from the main flow and create aerodynamic losses. Second, their rotation can bring the hotter gas from the main passage to the endwall creating high heat transfer regions. **Medic and Durbin, 2002**, improved turbulent model (k- $\omega$ ,k- $\epsilon$ ,V<sup>2</sup>-f) that can be used in any particular application. This analysis is dealing with transonic compressible flow through a gas turbine blade cascade. The results showed that a good predictions for the case of using k- $\epsilon$  model. In all models, the turbulent intensity T<sub>u</sub> was high at the stagnation point and in the near wake region. **Galzada and Alonso,2003**, Investigated the mechanism of the flow and heat transfer in separated flows particularly in separation and reattachment points .Also, they studied the influence of inlet flow angle, Reynolds number, Mach number on the heat transfer mechanism. The result showed that both the local Stanton number and the local heat transfer coefficients drop approaching the separation point and rose rapidly up to the region where flow reattaches. **Saha and Acharya,2008**, Investigated the modification design of endwall for reduction of heat transfer and total pressure losses .Various non-axisymmetric endwalls were studied using three-dimensional numerical simulations .The results showed that the total pressure loss was also low and the average heat transfer reduced by about 8% compared to the flat endwall. Local reduction in heat transfer was significant. **Sonoda et al, 2009**, Investigated the effect of three types endwall contouring: 1 only hub contour 2 only tip contour 3 hub and tip contours on the aerodynamic performance for the low -aspect ratio transonic turbine inlet guide vane IGV. Also they investigated the secondary flow mechanisms to show whether there were difference between the secondary flow models. The result showed that all types of endwall contouring reduce the mass averaged

overall loss by 4% for type 1, 5% for type 2 and 10% for type 3 as compared to the base line. Also, the flow mechanism in the small size full annular ultralow -AR transonic turbine IGV was different from the secondary flow model obtained from the low speed linear cascade.

There were some researches available on modification of endwall junction flow by passive modification to control flow by using fillet upstream leading edge and three-dimension 3D endwall contour, But a few researches were found on modification of the junction flow using riblet upstream leading edge. Based on the past studies, there is a clear need to investigate further the secondary flow losses and heat transfer characteristic of the endwall junction of a modern day stator vane.

The present work aims to explore concept of weakening the secondary flows and reducing their harmful effects by using a numerical technique to predicate the optimum dimensions of riblet by testing different riblet geometries. A theoretical formulation is used to examine secondary flow and drag reduction with longitudinal riblet upstream leading edge vane, by using the known package FLUENT version 12.1. Continuity and Navier -Stokes equations are solved in turbulent regime with an appropriate turbulent model SST,  $k-\omega$  in three-dimension. Numerical solution will be carried out for 25 riblet models type V-groove with various riblet heights, spaces and geometries on junction flow.

## 2. COMPUTATIONAL ASPECTS

An accurate simulation of flow over riblet required that each riblet cross-section be represented by at least several grid points in addition to accurately simulate analysis. The turbulent flow passage width and length should be greater than the size of characteristic turbulent flow structure such as boundary layer streaks and quasi-stream wise vortices. All this parameters are taking into the consideration in simulation process. The model facility is shown in **Fig. 2** and consists of one passage between two adjacent vanes. The model consists of inlet section, vane endwall junction hub, outer endwall junction casing and outlet section. The inlet section is located at one chord length upstream of airfoil leading edge, while the outlet

section at one chord length downstream trailing edge.

### 2.1 Vane Airfoil and Riblet Geometry

The airfoil profile of guide vane of gas power plant Unit PG9171E is found by using **Gambit** program, as shown in **Fig. 3**, with the dimensions as given in **Table 1**. The riblets types V-riblet with different dimensions are used in the present work and found by using **Gambit** program as given in **Table 2**.

### 2.2 Mesh Topology

For unstructured mesh, FLUENT uses unstructured solver with internal data structures to assign an order to the cells, faces, and grid points in a mesh and to maintain contact between adjacent cells. This gives the flexibility to use the best grid topology for complex geometry. The solver does not force an overall structure or topology on the mesh (i.e., it does not require i, j, k indexing to locate neighboring cells). FLUENT code uses different element types for mesh topology. The type of element specifies the number of mesh nodes and the node pattern associated with element shapes.

The model will be meshed by using tetrahedral element as shown in **Fig.4**. Although many mesh generation codes, Fluent & Ansys, support mesh generation of solid geometry and three-dimensional models from a single phase with minimum input the user **Fig. 5**, but it is more durable to divide this process into subsequent steps including two major issues for further controlling of the mesh, and are as follows:-

#### (I) Surface mesh generation:

Surface mesh is created for the vane-endwall junction geometry including the riblet, airfoil, and other boundaries as follows:

- Edges are meshed by assigning an interval size for each boundary comprising a closed loop of area.
- Edges meshes are controlled by specifying a grading scheme for each individual edge.
- Once all edges are meshed, a triangular element is used to generate a three-dimensional pave unstructured surface mesh.

#### (II) Volume meshes generation:

As far as all surfaces for each individual area have been meshed, volume mesh can be created for each zone comprising a closed loop

of area using T-Grid, **Gambit** scheme .Building the mesh required fine cells in area near the riblet , vane and endwall junction surface ,so that it is convenient for turbulent flow characterized with wake and separation .Therefore ,the mesh should be manipulated and controlled manually to keep smooth mesh transition and maintain accurate mesh for a three-dimensional model with a minimum computational expense .This was achieved by applying the size function.

Size functions are used to control the size of mesh intervals for edge and mesh elements for faces or volumes and thus to keep smooth transition of mesh from fine mesh near the nozzle vane-endwall junction surface to coarse mesh far away at the undisturbed boundaries .

### 2.3 Computational Method

In order to examine secondary flow and drag reduction, continuity and Navier-Stokes equations will be solved by using the known package FLUENT version 12.1. Continuity and Navier –Stokes equations are solved in turbulent regime with an appropriate turbulent model SST, k- $\omega$  in three-dimension .Numerical solution will be carried out for 25 riblet models type V-riblet with taking into account the effect of riblet height ,space and geometry on junction flow.

#### A-Flow Field Characteristics:

The most important aerodynamic characteristics in this study are drag, local skin and static pressure coefficients, turbulent intensity and secondary flow.

•Drag coefficients are calculated as follows:

$$C_d = \frac{F}{1/2\rho U_\infty^2} \quad (1)$$

Where F is the resultant force and divided into two components,

- 1-Pressure force acts on airfoil and riblet.
- 2-Viscous force acts on airfoil, riblet, bottom endwall junction hub and outer endwall junction casing.

•Local skin –friction coefficient ( $C_f$ ). **Calzada and Alonso, 2003.**

$$C_f = \frac{\tau_w}{1/2\rho U_\infty^2} \quad (2)$$

•Static pressure coefficient ( $C_p$ ). **Barringer and Thole, 2009.**

$$C_p = \frac{(P_{stat} - P_{stat,ref})}{1/2\rho U_\infty^2} \quad (3)$$

•Turbulent intensity

$$T_u = \frac{u_{rms}}{U} \quad (4)$$

•Secondary flow formation

The average secondary kinetic energy of the secondary flow is defined as: **Aunapu et al, 2000.**

$$SKE = \sqrt{v^2 + w^2} \quad (5)$$

#### B- Heat Transfer Characteristics:

The most important heat transfer characteristics in this research are the Stanton number and Nusselt number.

•Stanton number is calculated as follows. **Levchenya, 2007.**

$$St = \frac{h_c}{\rho C_p U_\infty} = \frac{q_w}{\rho_{ref} U_\infty C_p (T_w - T_\infty)} \quad (6)$$

•Nusselt number ( $N_u$ ) is given by: **Barringer and Thole, 2009.**

$$N_u = \frac{h_{local} \times C_{ax}}{k_f} \quad (7)$$

## 3. RESULTS AND DISCUSSION

### 3.1 Selection the Best Model of Riblet

The effect of riblet ratio h/s on drag reduction behavior for V-groove riblet models

are presented in **Figs. 6 up to 10**, taking into account the effect of riblet spacing and height as in **Table 2**. Peak angles for riblet model are selected based on data given by, **Stalio and Nobile, 2003**.

Generally, as shown in figures that the riblet at upstream leading junction has an effective upon drag reduction. Drag reduction occurs for all V-riblet models. The trend of increase in total drag can be attributed to an increase of effectiveness of riblet in adverse pressure gradient. Maximum drag reduction occurs at riblet model with peak angle of  $80^\circ$  and ratio of  $h/s=0.595$  for all ranges of  $h$  1-2mm. The models number Mo.2, Mo.7, Mo.12, Mo.17 and Mo.22, have the most effect in reduction of drag and heat transfer upon the others as shown in **Table 3**. One can find that, all these models have an effect on heat transfer reduction. Behavior of drag and heat transfer reduction are shown in **Fig.11** and indicates that, Mo.12 and Mo.17 are the most effective on drag and heat transfer reductions.

The selection of optimum dimensions are based on a maximum drag reduction and acceptable heat transfer reduction, therefore Mo.12 is considered to be the best model. It is manufactured to present the structure of flow field. The drag results indicate that there are an average skin-friction reduction for V-groove riblet model which has a specified dimensions of space  $s$  and height  $h$ .

### 3.2 Structure of Flow Field

#### 3.2.1 Structure of flow field at leading edge endwall junction

The velocity vectors, streamline pattern, velocity gradient and secondary flow contour and vector in the same flow domain of interest are presented in **Figs. 12,13,14,15** and **16**. The velocity vectors in **Fig. 12** are parallel to each other in the region far away from the base wall indicating a uniform incoming flow. As the endwall boundary layer approaches vane, the flow stagnates as shown in **Fig.13**. The fluid velocity increases with distance from endwall, this creates a static pressure gradient along the span. In other words, a pressure difference exists in the spanwise direction and a minimum static pressure exists at the endwall. The streamline

patterns and velocity gradient at the leading edge as shown in **Figs.14** and **15** illustrate how the free stream and near wall fluid migrates toward the endwall junction as a result of the relatively low static pressure which exists at junction. In addition, the streamlines close to the endwall demonstrate that the incident flow, first turns towards the wall then reverses and moves upstream. This explains the origin of the circulation associated with the horseshoe vortex system. The relationship between the axial velocity and secondary flow can be characterized by pumping action of the mean horseshoe vortex structure at work. The mechanism which brings the high momentum fluid into the junction and ejects low momentum from the near wall region can be shown in **Fig.16** at a region approximately 32%  $H$  of the span height and 35%  $C_{ax}$  upstream of the leading edge near van-wall interaction. The flow is directed outward from the vane with negative flow angle, then changes direction of the secondary flow with positive flow towards the vane to base which resulted in clockwise vortex. The secondary flow structure near the base wall, tends to be flattened into an elliptical shape and the contribution of velocity  $V_y$  at pitchwise in secondary velocity is larger than the velocity  $V_z$  at spanwise resulting clockwise motion. In that region, the horseshoe vortex wraps around the leading edge and splits into two legs, first leg of horseshoe vortex moves toward the pressure side of the vane and second moves toward the suction side of the vane and is called the suction side leg.

#### – Effect of riblet on the secondary flow structure

The effect of riblet on leading edge are shown in **Figs. 17,18,19** and **20**. The position of saddle point moves toward the leading edge as shown in **Fig. 18** and separation line pattern is different. Since the region between the saddle point and the leading edge where the flow separates to yield horseshoe vortex is short for the riblet wall, this implies that the size and extent of the leading edge horseshoe vortices are small for riblet case. The orientation of the streamlines for the riblet changes in flow direction and this is not the case for the smooth surface. Thus yaw angle of the flow near the wall will be reduced as shown in **Fig.19** which

in turns will reduce the development of the passage vortex. Also, the riblet reduces the size of secondary flow vortex and with a velocity gradient at endwall as shown in **Fig. 20**.

### 3.2.2 Pressure distribution at endwall

Static pressure coefficient distributions at endwall (hub) around the vane surface from the leading edge to the trailing edge are presented in **Figs. 21 and 22** with and without riblet surface modification of leading edge. Near the endwall, the flow is complex, being affected by the interaction of plate and vane boundary layers and by the horseshoes vortex.

As shown in figures, the minimum pressure occurs on the suction side due to the high fluid acceleration on this side. While the maximum pressure occurs on the pressure side due to the low fluid velocity on this side. Therefore, there is a pressure gradient from pressure side towards the suction side, which result in cross flow from pressure side to suction side of passage and this cross flow increases the formulation of secondary flow. The negative values of pressure coefficient extends to the suction side reaches to the lower with a value of -5.5 in the throttle region at  $X/C_{ax}=88\%$  till trailing edge. The positive values of pressure coefficient extends near the pressure side then changes its sign to a negative. Also, there is a reduction in the wake region reaches up to the value of -4.5. The higher negative value of pressure coefficient in the center of passage vortex results in a peak turbulent kinetic energy.

In the passage, there is a minimum static pressure location a long suction surface of the vane and an attenuated suction side leg of the horseshoe vortex still exists. A high magnitude value of the loss coefficient in the suction side and trailing region of vane reaches up to a wake region. It can be observed that a strong adverse pressure gradient upstream at vane leading edge causes flow separation in this region.

#### - Effect of riblet on pressure coefficient, $C_p$ distribution at endwall junction

From **Fig.22** it can be seen that, the pressure coefficients with the riblet are greater in magnitude than the corresponding points without riblet. There are an increase in pressure

coefficient in the region very close to leading edge endwall junction. It seems that, when the riblets are placed in the location of the separation point on the endwall surface, there is an increase in momentum in this region. The stagnation streamlines move to location closer to leading edge resulting in an increase in momentum in the corner, also, with riblet less pressure losses occurs across the passage. Reduction in pressure gradient from pressure side to suction side leads to reduction in cross flow, where a maximum reduction occurs in throttle region.

### 3.3 Structure of Heat Transfer.

#### 3.3.1 Heat transfer distribution at leading edge

The leading edge of vane experiences very high load, there are some regions with a higher heat transfer than others. **Fig. 23** illustrates the distribution of Stanton number at the leading edge junction flat plate endwall junction. Stanton numbers begins to increase dramatically at a location upstream of the leading edge vane approximately 15% of the chord  $X/C_{ax} = -0.15$ . It is related to the position where the flow separates from the endwall, which occurs at approximately  $X/C_{ax} = -0.12$ , the heat transfer continues to increase till the flow approaches the vane. The leading edge and endwall platforms of the vanes are areas with highest thermal loads for two reasons; firstly, the vertical flows increase the transport of relatively hot flow from the mid-span towards the endwall juncture. Second, because the platform is affected by secondary flows, it experiences an increase in heat transfer coefficients, **Radomsky and Thole, 2000**. Stanton number levels decrease as the thermal boundary layer thickens and then increases as the stagnation region is approached. The high heat transfer rates in this region are consistent with the horseshoe vortex, where formulation of vortex system in this region increases with mixed process. The trend of the results was in consistent with measurement of **Radomsky and Thole, 2000**.

One can notice that, the high heat transfer regions at leading edge with the stagnation region near leading edge of the vane, the highest

Stanton number values occur nearest to the vane surface. This peak value occurs because the secondary flows bring the high speed mainstream fluid down towards the endwall, thereby thinning the boundary layer.

### —Riblet effects on the heat transfer structure

Fig. 24 shows the main effect of riblet sheet at upstream vane on distribution of heat transfer. The figure shows that the location of very hot spots is shifted away from leading edge to another location in the passage that lead to weaken the heat load on the front of leading edge. The riblet controls the flow direction through reducing the turning angle of hot stream toward the endwall. Reduction in heat transfer rate in the leading edge and endwall is obtained by using of riblet surface.

### 3.3.2 Endwall junction heat transfer distribution

#### -Stanton number, (St) distribution at endwall

The heat transfer coefficients given in Fig. 25 represents in terms of a non-dimensional Stanton number  $st \times 1000$ . In the region upstream of the vanes, a high heat transfer region is occurred between the stagnation point and the reattachment point of the flow on the suction side of the airfoil where the Stanton number is reached to the value of 4.5. This is the area which experiences a very high acceleration. But the local Stanton number drops approaching the separation point, as the flow moves through the passage. It is apparent that the location of the peak Stanton numbers peak heat transfer is being swept from the outer pressure surface towards the suction side of the central vane causes high heat transfer along the suction side of vane. The favorable static pressure gradient, which moves away from the stagnation region and the pressure surface, tends to drive the separation line for the inlet boundary layer toward the suction surface.

This lowest heat transfer region is contained with the convergence of the separation streamline from suction surface leg of the horseshoe vortex and the separation streamline due to the roll up of the pressure

surface leg of the horseshoe vortex by the passage vortex.

Downstream from the trailing edge of the vanes, the influence of the wake is appeared on the endwall heat transfer with lower value on the pressure surface than the trailing suction surface.

#### - Riblet effect on Stanton number, (St) distribution

Fig. 26 illustrates the effect of riblet on distribution of Stanton number on endwall junction. With riblet surface, the distribution of Stanton number changes upstream of leading edge where the riblet surface has low heat transfer rate which leads to decrease heat transfer in region very close to leading edge endwall junction. The riblet shifts the location of high heat transfer to points furthest from junction. High heat transfer rates are still presented in the stagnation region and downstream from the trailing edge of the vane but the effect of the separation streamline is not apparent.

## 4. CONCLUSIONS

1-The effect of secondary flow on endwall junction flow extends up to 23% $H$  from span height and 35 %  $C_{ax}$  upstream leading edge.

2-The drag reduction produced by riblet is proportional to their sizes. These sizes represent height  $h$ , space  $s$  and riblet cross-section area.

3- The maximum drag reduction obtained is 2.7% for the V-groove riblet type which has a height  $h=1.35$  mm, space  $s=2.26$ mm and peak angle of  $80^\circ$ . The other sizes have lower drag reduction.

4-The effect of riblet causes a reduction of secondary flow formation in the region very near to the endwall junction as well as a reduction in the average of secondary flow formation near pressure side.

5-Significant effects of riblet endwall on pressure distribution in hub from leading edge to trailing edge are observed. The riblet reduces cross-flow from pressure side to suction side and leads to weaken of secondary flow formation.

6- With riblet there is an increase in momentum in the region very close to leading edge endwall junction in turn leads to move stagnation point to location close to leading edge.

7- A maximum reduction in average heat transfer near the leading edge-endwall juncture is obtained. The riblets shift the location of high heat transfer to upstream furthest from junction. While; a little reduction is obtained in the downstream portion of the passage.

8- The amount of heat transfer reduction in the leading edge is due to reduction in secondary flow formulation at leading edge junction.

9- The riblet surface controls the flow direction in the boundary layer and reduces the thickness of boundary layer by increasing the momentum in streamwise direction.

### 5- Nomenclatures

$C_{ax}$  axial chord (mm)  
 $h$  local heat transfer coefficient .  
 $I$  current (A).  
 $K_s$  surface thermal conductivity .  
 $k-\omega$  turbulent model.  
LDV laser Doppler velocimeter.  
 $R$  Reynolds number.  
SST shear stress transport.  
 $T_\infty$  local free stream temperature (K).  
 $T_w$  local wall temperature (K).  
 $u$  axial velocity component in X-direction (m/s).  
 $U_\infty$  free stream velocity (m/s).  
 $V$  voltage (V).  
 $\rho$  density ( $\text{kg/m}^3$ ).  
IGV Inlet guide vane.  
 $C_d$  drag coefficient .  
 $C_f$  skin- friction coefficient  
 $\tau_w$  wall shear stress.  
 $C_p$  static pressure coefficient .  
 $T_u$  turbulent intensity (%)  
 $q_w$  wall heat flux.

### 6- REFERENCES

Calzada P.D.L, and Alonso A, 2003, *Numerical Investigation of Heat Transfer in Turbine Cascades with Separated flows* ASME, Journal of Turbo- Machinery , Vol.125, April.

Medic G., and Durbin P.A, 2002, *Toward Improved Prediction of Heat Transfer on Turbine Blades*. ASME, Journal of Turbo- Machinery , Vol. 124, PP 187, April.

Program, 2009, *Ansys CFX, Version 12* Ansys Inc.,.

Program ,2009, *Tecplot 360, version 12.0.0.3116"*, Tecplot Inc.

Radomsky R.M. and Thole K.A, 2000, *Flow Field Measurements for a Highly Turbulent Flow in a Stator Vane Passage*. ASME, Journal of Turbomachinery, Vol.122, April.

Radomsky R.M. and Thole K.A, 2000, *High Free-Stream Turbulence Effects on Endwall Heat Transfer for a Gas Turbine Stator Vane*. ASME, Journal of Turbo-Machinery, Vol.122, October ,2000.

Saha A.K and Acharya S 2008, *Computation of Turbulent Flow and Heat Transfer through a Three-Dimensional Nonaxisymmetric Blade Passage*. ASME, Journal of Turbo- Machinery, Vol. 130/031008-1, July..

Sonoda T., Hasenjäger M., Arima T. and Sendhoff B, 2009, *Effect of Endwall Contouring on Performance of Ultra-low Aspect Ratio Transonic Turbine Inlet Guide Vanes* ASME, Journal of Turbo Machinery, Vol. 131, January.

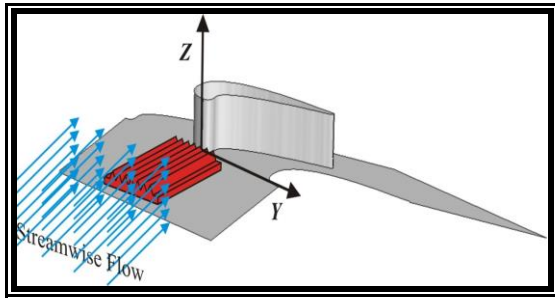


Figure 1. Position of leading edge riblet.

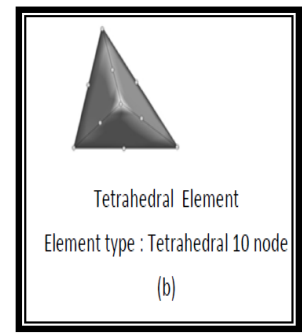
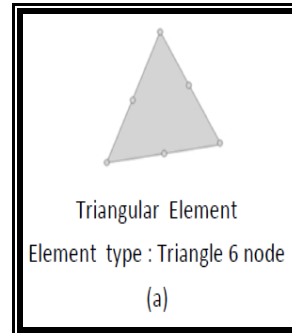


Figure 4. (a) Triangular elements type, (b) Tetrahedral elements type.

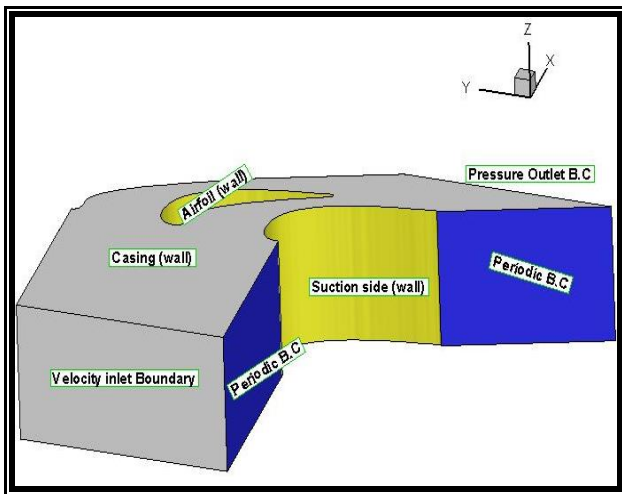


Figure 2. Facility of model with one passage on inlet guide vane.

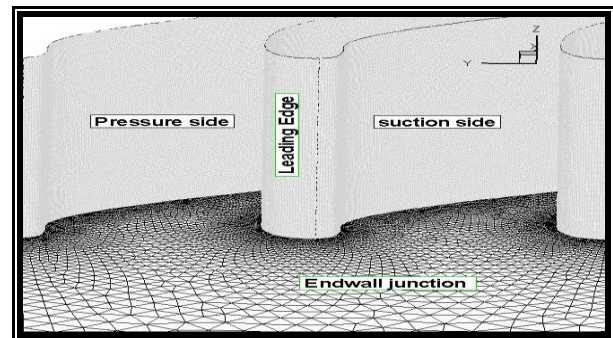


Figure 5. Fine mesh near the nozzle vane-endwall junction surface.

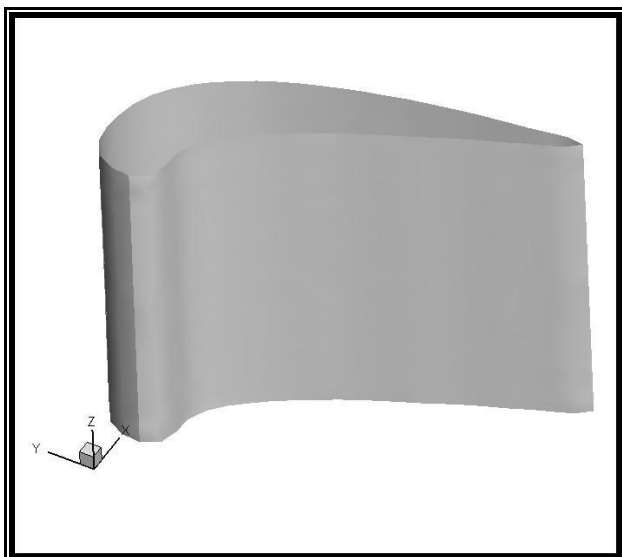
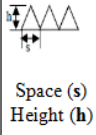


Figure 3. Vane airfoil profile by use of Gambit program.

**Table 1.** Dimensions of guide vane of gas power plant (unit PG9171E).

1	Span or vane height (H)	210 mm
2	Pitch or vane spacing (S)	175 mm
3	Chord length (C)	280 mm
4	Axial chord length ( $C_{ax}$ )	145.12 mm
5	Inlet flow angle ( $\beta_1$ )	0° degree
6	Outlet flow angle ( $\beta_2$ )	72.8° degree
7	Stagger angle ( $\lambda$ )	56.4° degree
8	Inlet velocity ( $U_{ref}$ )	19 m/s
9	Inlet turbulent Intensity ( $T_u$ )	3.0 %
10	Chord Reynolds number (Re)	$3.38853 \times 10^5$
11	Length of suction side (L <sub>ss</sub> )	334 mm
12	Length of pressure side (L <sub>ps</sub> )	275 mm

**Table 2.** Riblet models dimensions.

Riblet configuration	Model No.	Height (h)mm	Peak angle ( $\theta$ )degree	Space (s)mm	Ratio h/s
 Space (s) Height (h)	Mo.1	2.00	90	4.00	0.500
	Mo.2	2.00	80	3.35	0.595
	Mo.3	2.00	70	2.80	0.714
	Mo.4	2.00	60	2.30	0.869
	Mo.5	2.00	53	2.00	1.000
	Mo.6	1.68	90	3.36	0.500
	Mo.7	1.68	80	2.82	0.595
	Mo.8	1.68	70	2.35	0.714
	Mo.9	1.68	60	1.94	0.869
	Mo.10	1.68	53	1.67	1.000
	Mo.11	1.35	90	2.70	0.500
	Mo.12	1.35	80	2.26	0.597
	Mo.13	1.35	70	1.89	0.714
	Mo.14	1.35	60	1.55	0.871
	Mo.15	1.35	53	1.35	1.000
	Mo.16	1.23	90	2.45	0.500
	Mo.17	1.23	80	2.10	0.595
	Mo.18	1.23	70	1.72	0.714
	Mo.19	1.23	60	1.42	0.860
	Mo.20	1.23	53	1.22	1.000
	Mo.21	1.00	90	2.00	0.500
	Mo.22	1.00	80	1.67	0.595
	Mo.23	1.00	70	1.40	0.714
	Mo.24	1.00	60	1.15	0.860
	Mo.25	1.00	53	1.00	1.000

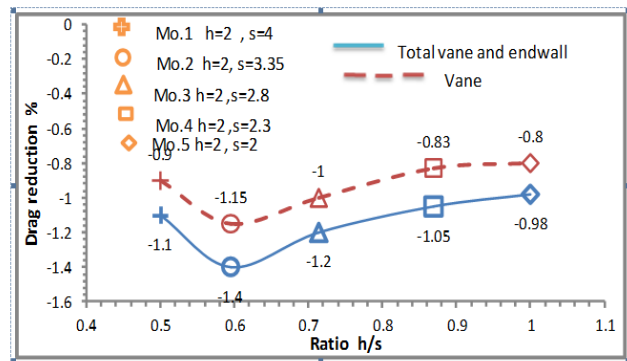


**Figure 6.** Drag reduction for different ratio h/s at (h=2mm).

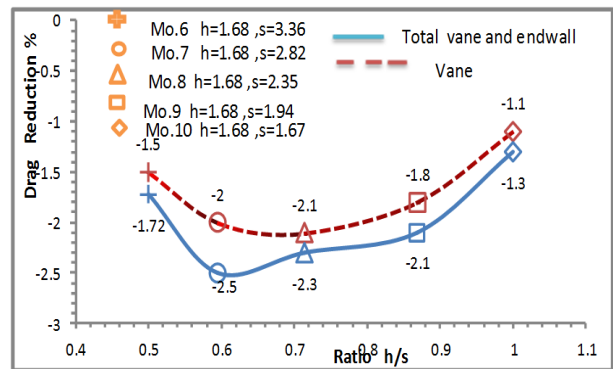


**Figure 7.** Drag reduction for different ratio h/s at (h=1.68mm).

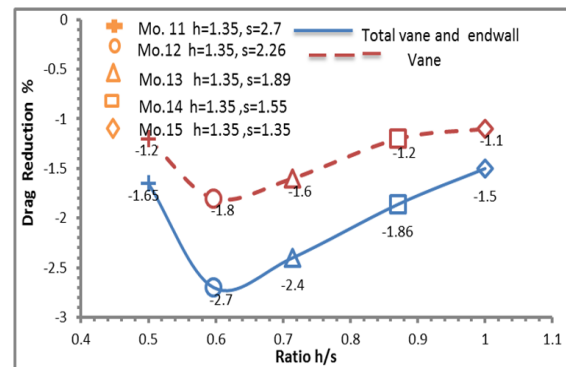


**Figure 8.** Drag reduction for different ratio h/s at (h=1.35mm).

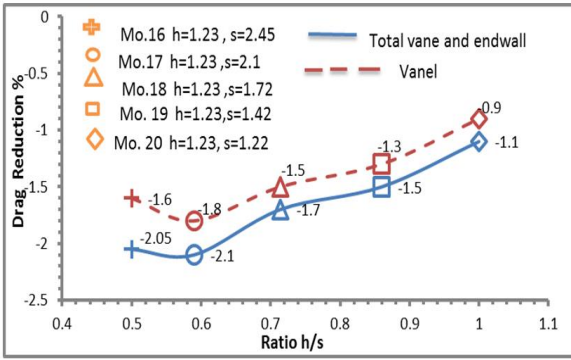


Figure 9. Drag reduction for different ratio (h/s) at (h=1.23mm).

Table 3. Maximum effect of riblet on drag and heat transfer at peak angle(80°).

Model No.	Height (h mm)	Space (s mm)	Ratio h/s	Airfoil drag reduction %	Total drag reduction (DR) %	Total Stanton number reduction (st ×1000)%
Mo.2	2.00	3.35	0.595	-1.15	-1.40	-18.0
Mo.7	1.68	2.82	0.595	-2.00	-2.55	-21.4
Mo.12	1.35	2.26	0.595	-2.15	-2.70	-21.0
Mo.17	1.23	2.10	0.595	-1.70	-2.10	-23.0
Mo.22	1.00	1.67	0.595	-1.73	-2.20	-20.8

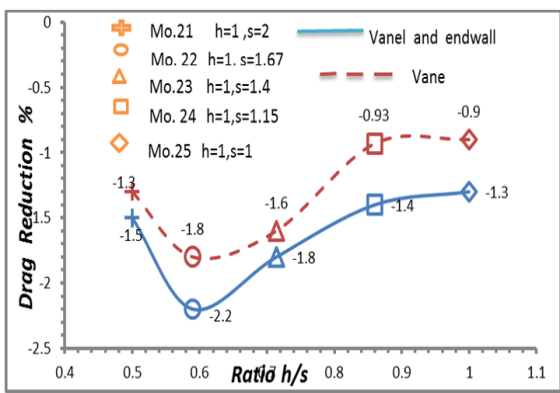


Figure 10. Drag reduction for different ratio (h/s) at (h=1mm).

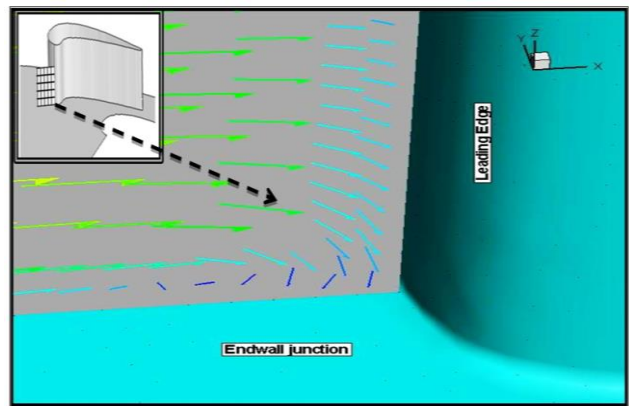


Figure 12. Velocity vector at the leading edge endwall junction without riblet.

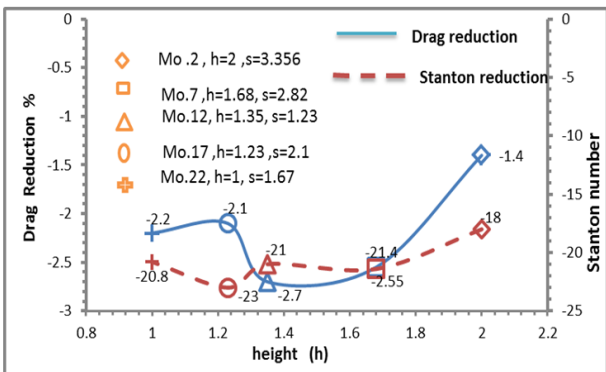


Figure 11. Drag and heat transfer reduction of riblet surface.

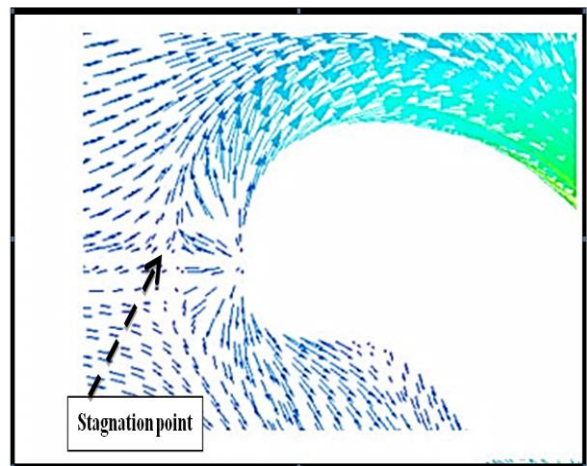


Figure 13. Velocity vector at the leading edge.

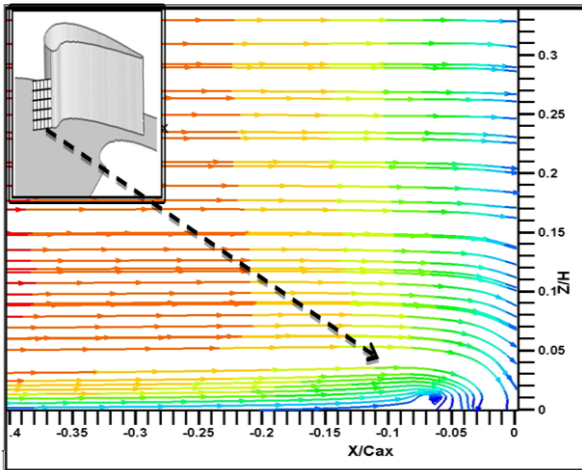


Figure 14. Streamline show horseshoe vortex at the leading edge junction without riblet.

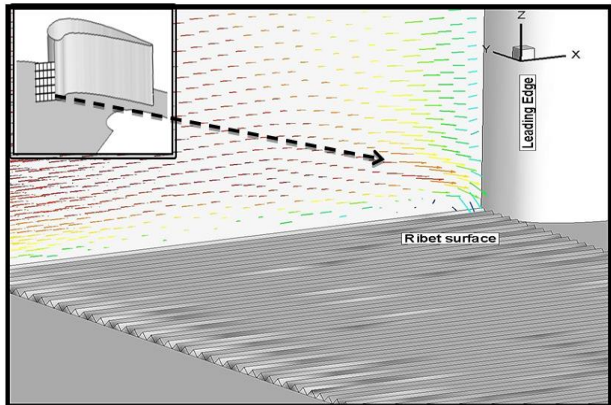


Figure 17. Velocity vector at the leading edge endwall junction with riblet.

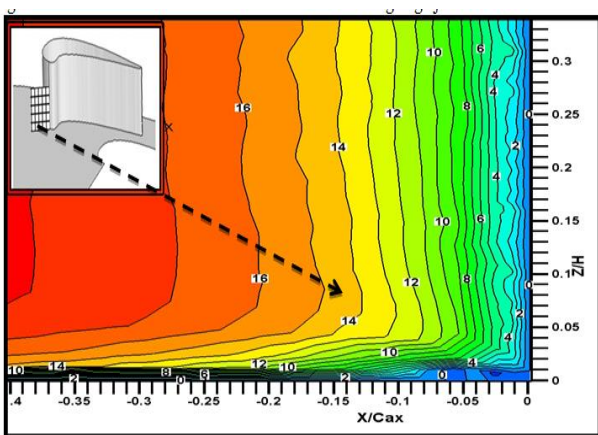


Figure 15. Velocity contour at the leading edge junction without riblet.

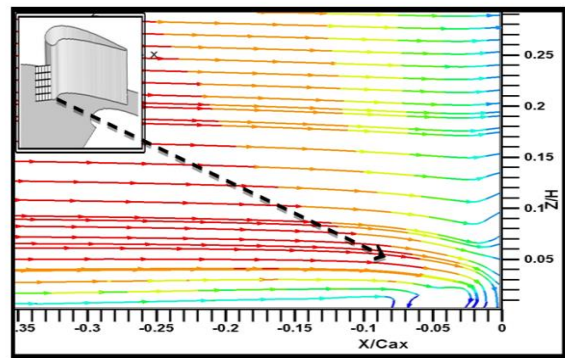


Figure 18. Horseshoe vortex at the leading edge junction with riblet.

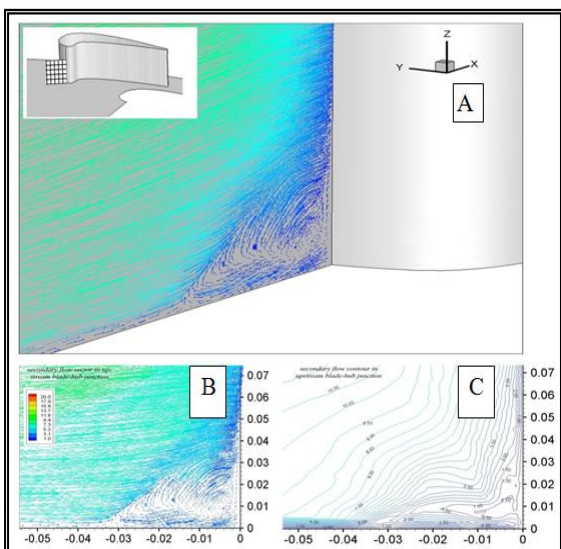


Figure 16. Secondary flow vector and contour in upstream vane-hub junction.

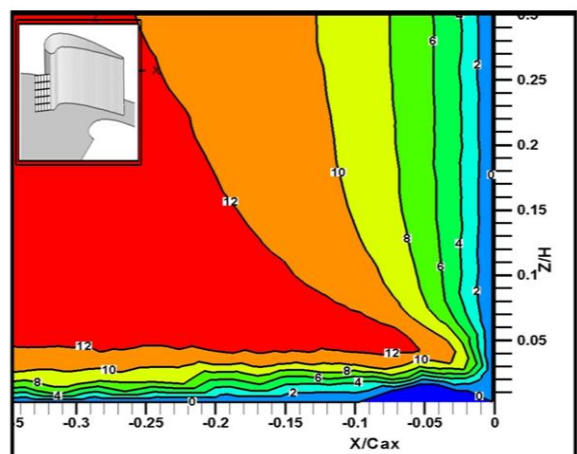
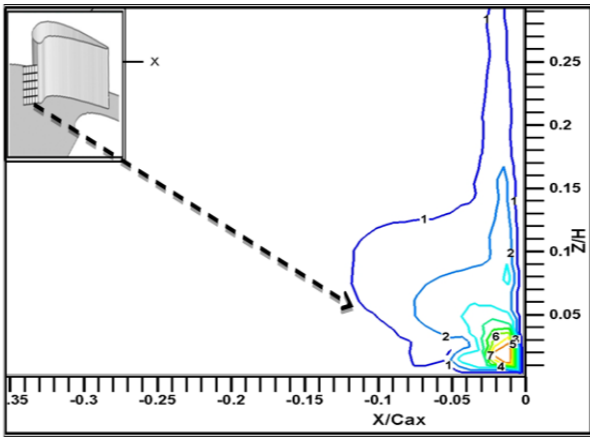
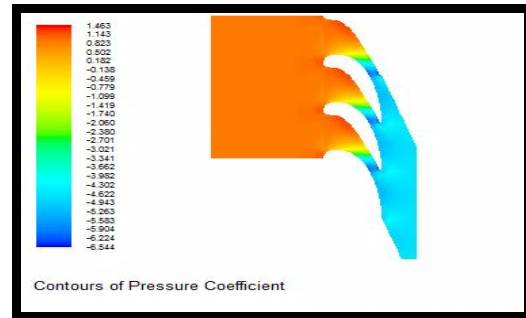


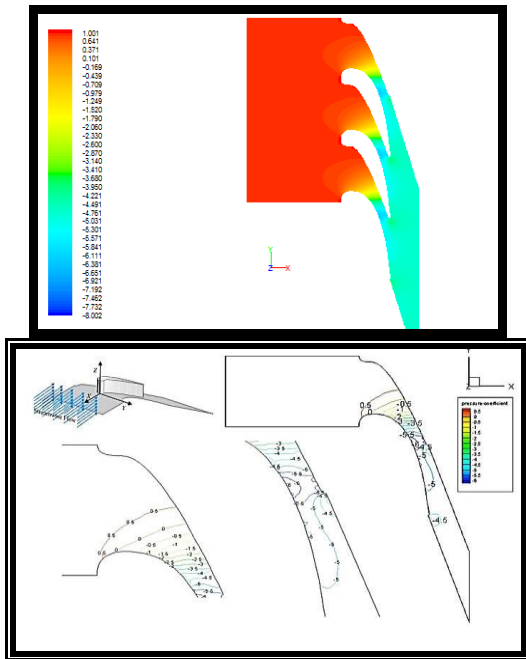
Figure 19. Velocity contour at the leading edge junction with riblet.



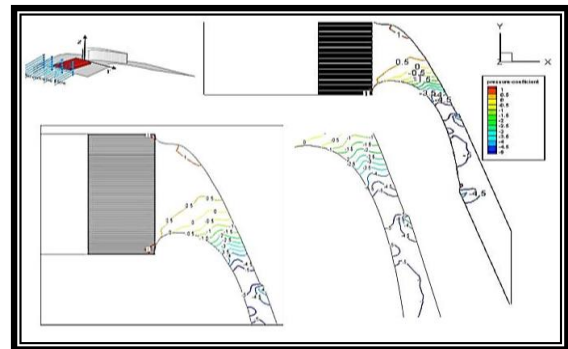
**Figure 20.** Scondary flow vector and contour in upstream vane endwall junction.



**Figure 22.** Contour of static pressure coefficient distribution on the endwall junction for gas turbine nozzle guide vane with riblet upstream leading edge. A-Filled contour, B-Line contour.



**Figure 21.**Contour of static pressure coefficient distribution on the endwall junction for gas turbine nozzle guide vane without riblet. A- Filled contour, B-Line contour.



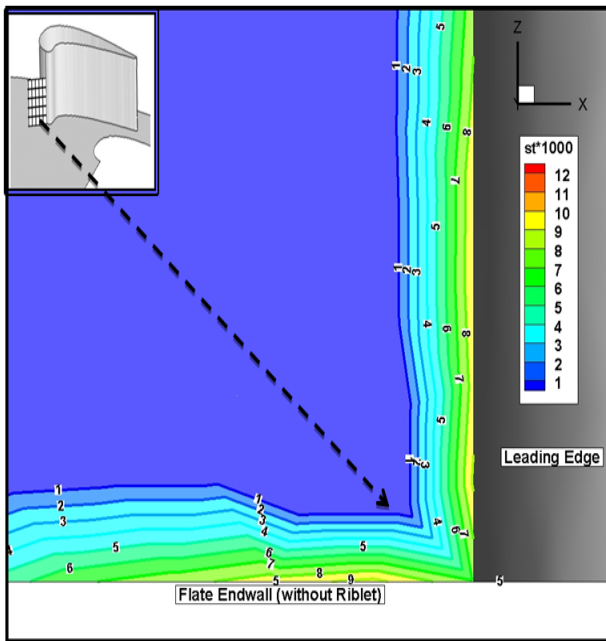


**Figure 23.** Stanton number distribution at the leading edge without Riblet.

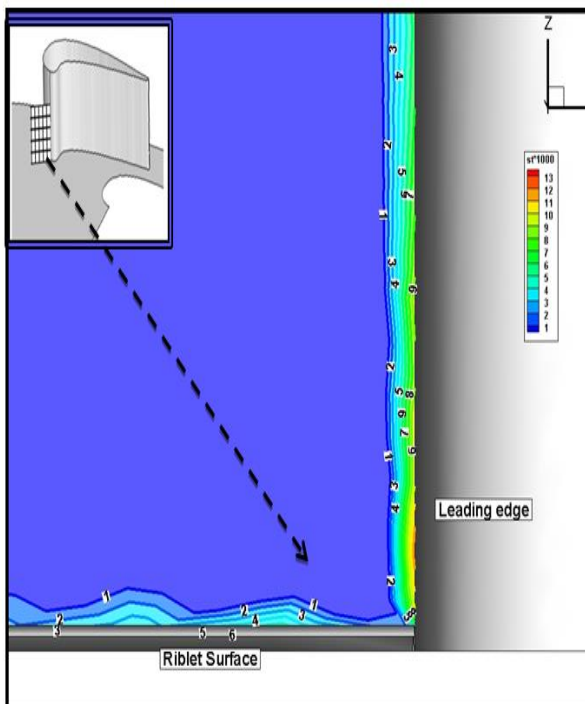


**Figure 24.** Stanton number distribution at the leading edge with Riblet.

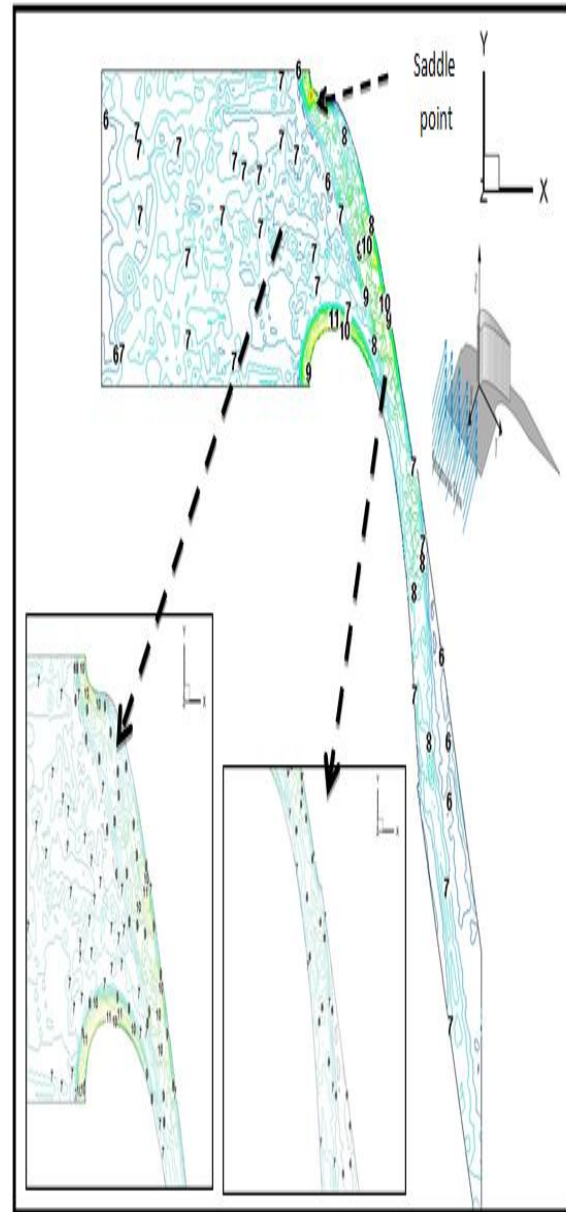


**Figure 25.** Stanton number distribution on the endwall junction without riblet.

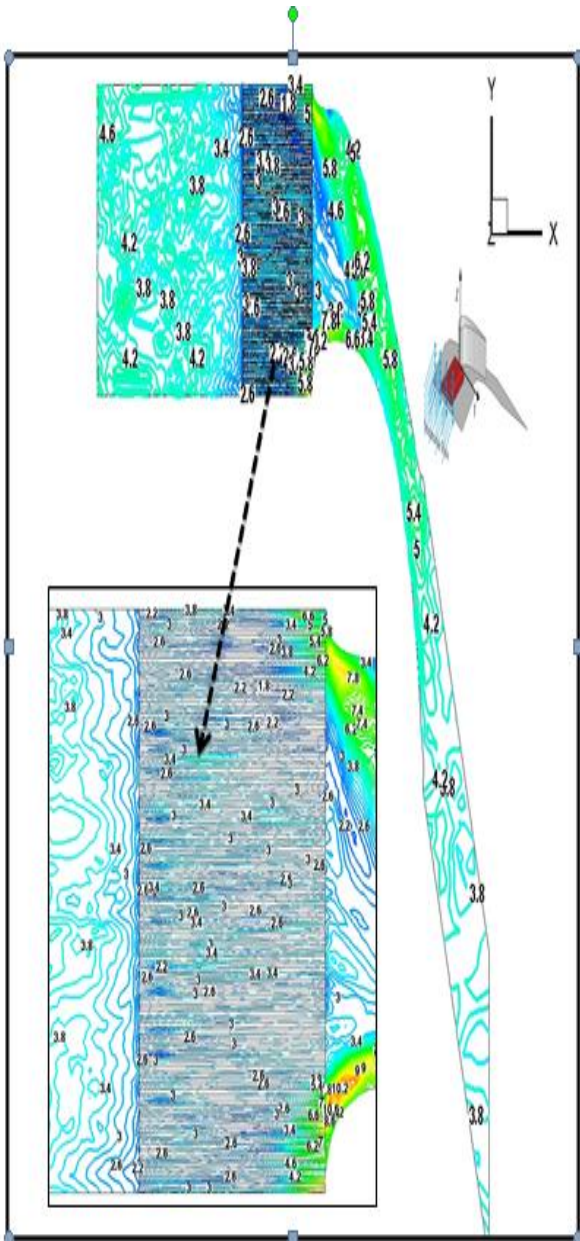


**Figure 26.** Stanton number distribution on the endwall junction with riblet.